The Solution Structure of Oxidized HiPIP I from *Ectothiorhodospira halophila*; Can NMR Spectroscopy Be Used to Probe Rearrangements Associated with Electron Transfer Processes?

Ivano Bertini,* Lindsay D. Eltis, Isabella C. Felli, Dieter H. W. Kastrau, Claudio Luchinat, and Mario Piccioli

Abstract: In the ^{1}H NMR spectrum of the oxidized form of the high-potential iron–sulfur protein (HiPIP I) from *Ectothiorhodospira halophila*, 91% of the total proton resonances and 100% of the residues have been assigned. The standard COSY, NOESY, and TOCSY sequences have been optimized for the paramagnetism of the molecule. Extensive assignment of the ^{15}N NMR spectrum has been obtained through HMQC spectra. With 1437 dipolar connectivities, of which about 10% involved fast-relaxing protons, a family of 18 structures was generated with an RMSD of 0.65 Å by using the programs developed by Wüthrich. The family of structures was further refined by various calculation steps; the final RMSD was 0.48 Å. The structures appear to be very similar but not equal to the structures of the reduced protein. Despite the similarity in structure, significant variations in the chemical shifts are observed. A similar behavior was observed for the homologous protein from *Chromatium vinosum*. It is concluded that NMR is a sensitive tool to monitor differences between oxidized and reduced proteins; however, the detailed structural variations should be evaluated with caution at the present level of resolution, which roughly corresponds to a resolution of 2.5 Å in an X-ray structure.

Keywords
electron transfer · iron–sulfur proteins · NMR spectroscopy · proteins · solution structures

Introduction

We have recently reported the solution structures of paramagnetic metalloproteins[1, 2] at a degree of resolution comparable to that observed for diamagnetic proteins of the same size.

Paramagnetism in general causes large proton chemical shifts and line broadening, and has for a long time prevented the determination of connectivities necessary for the solution of the structures of paramagnetic proteins. Our present interest lies in using the NMR technique to monitor structural rearrangements associated with electron transfer in metalloproteins. It is known that when the reorganization energy equals the free energy change, the electron transfer process between two redox pairs occurs at an optimal rate.[3, 4] We think that the comparison of both oxidized and reduced solution structures is quite instructive even if, in proteins devoted to electron transfer processes, only minor structural rearrangements are expected when passing from the oxidized to the reduced state and vice versa.[5] Moreover, at the present degree of resolution of the solution structures, which can be compared to a resolution in the solid-state structure of 2.5 Å,[6] the differences should be evaluated with caution. Our present strategy consists in refining the structures more and more precisely, on the one hand, and in extending the work to different but homologous redox proteins on the other. Bearing in mind that the solution structures of the reduced and oxidized high-potential iron–sulfur protein (HiPIP hereafter) from *Chromatium vinosum* are available,[2, 7] as well as the reduced structure of HiPIP I from *Ectothiorhodospira halophila*,[1] we report here the structure of the oxidized form of the latter protein.

HiPIPs contain the cubane-like Fe_4S_4 cluster,[8] which formally contains two Fe^{2+} and two Fe^{3+} in the reduced state and three Fe^{3+} and one Fe^{2+} in the oxidized state. Mössbauer studies have shown that the protein in its reduced state contains four $Fe^{2.5+}$ ions,[9, 10] and in its oxidized state two $Fe^{2.5+}$ and two Fe^{3+} ions.[9, 11] The rationale of these results is reported elsewhere.[12] In both oxidation states the protein is paramagnetic, although to a different extent. Recent evidence suggests that HiPIPs are involved in the electron transfer process of the photosynthetic center in photosynthetic bacteria.[13]

The results obtained allow us to compare 1) the structures of the oxidized and reduced forms of HiPIP I from *E. halophila* and 2) the common differences within the redox partners of the two HiPIPs. Until more refined structures are available, we can gain some insight into what happens to the structure when one electron is removed from or added to the cubane.

[*] I. Bertini, I. C. Felli, D. H. W. Kastrau, M. Piccioli
Department of Chemistry, University of Florence
Via Gino Capponi 7, I-50121 Florence (Italy)
Telefax: Int. code + (55)275-7555
L. D. Eltis
Department of Biochemistry, Université Laval
Quebec, G1K 7P4 (Canada)
C. Luchinat
Institute of Agricultural Chemistry, University of Bologna, (Italy)

0947-6539/95/0109-0598 $ 10.00+.25/0

Results and Discussions

Assignment: The ^{1}H NMR spectrum of the oxidized form of *E. halophila* HiPIP I spans over 110 ppm (Fig. 1 A); six (A–D, Y, and Z) out of eight β-proton signals are shifted well outside the diamagnetic region, and two of these (Y and Z) are upfield of the diamagnetic envelope.[14] The T_1 values of the βCH_2 protons are in the range of 3 to 12 ms. The hyperfine-coupled

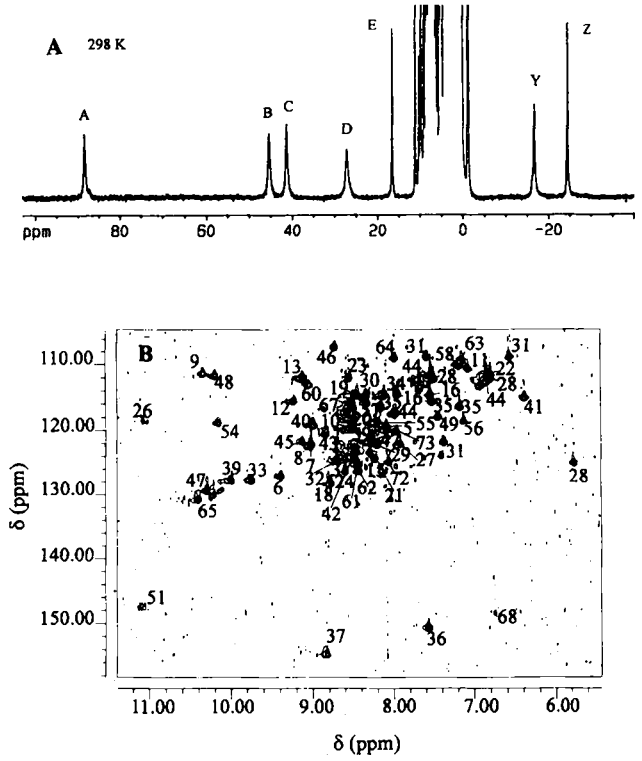

Fig. 1. A) ^{1}H NMR spectrum (600 MHz) of oxidized HiPIP I from *E. halophila*, at a pH of 5.0 and at 298 K. The seven signals A–E, Y, and Z correspond to the βCH_2 protons of three out of four Cys residues and to one, hyperfine-shifted Cys Hα (signal E). B) HMQC spectrum of oxidized HiPIP I from *E. halophila* (pH = 5.0, 298 K), recorded on a ca. 0.5 mM sample of uniformly ^{15}N-enriched protein. Peak numbering follows the residue number in the primary sequence.

signals βCH_2 and αCH of the Cys residues were assigned by analysis of the 1 D NOEs, by using spectra optimized to detect fast-relaxing signals, and by analysis of the 2D NOESY and TOCSY spectra recorded over the diamagnetic envelope. The detailed description of their assignment is reported elsewhere.[14] Nonselective T_1 values for cysteine protons are smaller in the reduced than in the oxidized form. Therefore, as far as nuclear relaxation is concerned, the oxidized protein is more suitable for NMR investigations than the reduced one. About 80% of the proton signals were assigned by comparing the maps of the reduced form with those of the oxidized form, as they were found to differ in chemical shift by less than 0.1 ppm. The other proton signals ($\approx$15%) were assigned following the usual strategy based on recognition of spin systems and on sequence-specific assignment.[15] In the oxidized form, it was possible to fully assign Asp 56 and Cys 36, residues that escaped detection in the reduced form. In total, the assignment was extended to 73 out of 73 residues.

HMQC experiments were performed (Fig. 1 B) to assign ^{15}N resonances by means of the assigned amide protons. With this procedure 76% of ^{15}N resonances could be assigned safely.

Calibration: The program CALIBA was used to integrate and calibrate the 3906 peaks in the 2 D NOESY spectra recorded at 288 K in H_2O and D_2O.[16] Dipolar connectivities were divided into the five different classes, described in the Experimental Procedure, and the calibration parameters were adjusted throughout the distance geometry (DG) calculations. In the final stages of the DG calculations, the best agreement between the NOESY intensities and the distances measured in the calculated structures was obtained by treating the volumes of cross peaks belonging to classes 1 and 5 to be proportional to $1/r^4$, those belonging to classes 3 and 4 to be proportional $1/r^5$, and those belonging to class 2 to be proportional to $1/r^6$. Proportionality to $1/r^6$ holds only for the limiting condition of a rigid structure. The use of exponents lower than 6 ($1/r^5$, $1/r^4$) was empirically introduced by Wüthrich and co-workers to better represent the relation between cross-peak volumes and upper-limit distances for peaks that involve side-chain protons.[16] The theoretical $1/r^6$ dependence does not hold if spin diffusion effects arise or if possible local motions decrease the reorientational correlation time.

A similar empirical approach was used to account for spin diffusion effects in calibrating the 1 D NOEs. For each of the seven hyperfine-shifted cysteine signals, as well as for Thr 51 HN and Val 68 γCH_3 signals, 1 D NOE spectra recorded with different irradiation times (20 or 40 ms, 60 or 100 ms, and 170 ms) were compared in order to discriminate amongst three classes of NOEs: 1) first-order NOEs (those visible with irradiation times of 20 or 40 ms); 2) NOEs that are slightly affected by spin diffusion, but that are not visible with short mixing times because of their very small intensity (60 or 100 ms); and 3) NOEs that are significantly affected by spin diffusion (170 ms). The intensities of the dipolar connectivities observed from each irradiated signal were converted into upper limits for the distance by using the proportionality of $1/r^6$, $1/r^5$, or $1/r^4$, depending on whether the NOE belonged to class 1), 2), or 3), respectively. This approach yielded 99 upper distance limits from 1 D NOEs. As with the 2D NOEs, calibration parameters were adjusted throughout the DG calculation, based on a comparison between the intensities of intraresidue dipolar connectivities and the distances in the calculated structures.

Structure calculation: The program DIANA was used for the preliminary examination of 1338 upper distance limits extracted from 2 D spectra together with 99 upper distance limits obtained from 1 D NOEs.[16] These constraints are summarized in Table 1. Of these, 340 were found to be irrelevant in that they could never be violated or arose from protons at fixed distances. A total of 1097 meaningful upper distance limits were retained in all subsequent calculations. The total number of observed NOEs per residue (intra and inter) and the effective number used in calculating the structure are reported in Figure 2. The cluster was simulated in the same way as in the reduced protein.[1] The four cysteine residues in the sequence were modified by substituting the thiol hydrogen with an iron atom at the

Table 1. Number of constraints constituting the upper-limit file.

1	intraresidue (except HN, Hα, Hβ)	312 (46 methyl peaks)
2	sequential and intraresidue HN, Hα, Hβ	380 (35 methyl peaks)
3	medium range	64 (8 methyl peaks)
4	long range, backbone	29
5	long range	553 (203 methyl peaks)
1 D NOEs	connectivities from 1 D NOE experiments	99

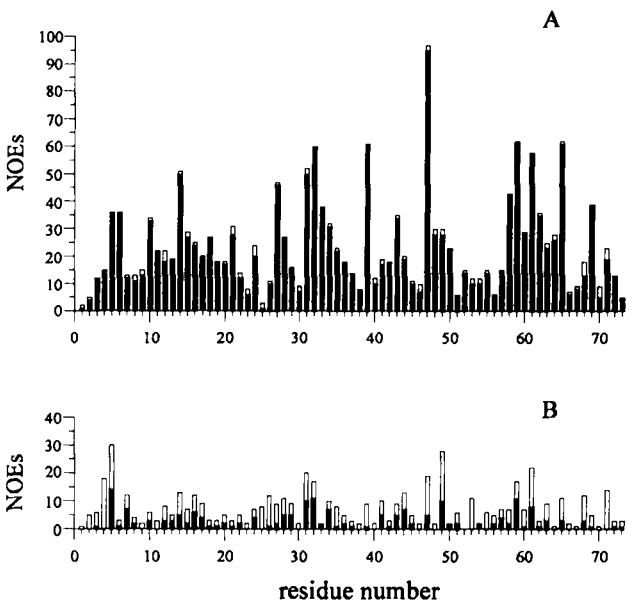

Fig. 2. Number of inter- (A) and intraresidue (B) NOEs for each residue. Only NOEs indicated with black columns were relevant for the determination of the solution structure.

appropriate distance and by attaching another sulfur atom to the latter. Upper and lower distance limits involving iron and sulfur atoms of different cysteines were introduced in order to simulate the correct geometry of the cluster. Bond lengths and angles for the modified cysteines as well as upper and lower distance limits were taken from known structures of Fe_4S_4 clusters.[17, 18] The REDAC strategy[19] was employed throughout the calculation, and 38 diastereotopic pairs were assigned stereospecifically by using the program GLOMSA.[16] A family of 18 structures, each with a target function lower than 0.4 Å^2, was obtained. Each structure in this family (DG family) was then energy-minimized (EM) and subjected to molecular dynamics (MD) simulations; this led to the restrained energy minimization (REM) and restrained molecular dynamics (RMD) families, respectively. The Fe_4S_4 cluster was included in MD calculations as an independent unit, bound to the protein through covalent bonds between iron and cysteine sulfur atoms. For the iron and sulfur atoms and for the iron-bound cysteines, previously reported force-field parameters were used.[20, 21] Finally the average structure from the RMD family was subjected to extended restrained molecular dynamics calculations in water, leading to the RMDw structure. The deviation from ideal angles and distances of RMDw are reported in Table 2; the maximal residual violation is 0.18 Å. The target function[16] for the DG family and the penalty function[22] for the REM and RMD families and for the RMDw structure (Table 2) are satisfactory.

Table 2. Average RMSD values for backbone (BB) and for all heavy atoms (HA) within the DG, REM, and RMD families. For the last two families the average energy is also reported. For the RMDw structure, the target function, the total energy, and two parameters indicating deviations from ideal geometry are reported.

	DG	REM	RMD	RMDw
BB (Å)	0.63±0.08	0.56±0.08	0.48±0.09	
HA (Å)	1.20±0.09	1.19±0.10	1.16±0.17	
target function (Å^2)	0.30±0.08			
target function (kJ mol^{-1})		49.75	49.37	34.26
energy (kJ mol^{-1})		−5033	−6569	−6206
deviation from ideal distances (Å)				0.008
deviation from ideal bond angles (°)				1.77

Description of the structure: The backbones of the DG, REM, and RMD families are shown in Figure 3. The overall resolution is good and, in most regions, improves progressively upon passing from the DG to the REM and to the RMD families. Other than the N and C terminal parts, the more disordered regions are those extending from residues 22–29 (lower loop) and 44–46 (upper left loop), which are relatively exposed to solvent. The average RMSD values over backbone atoms and all heavy atoms for each of the three families are reported in Table 2. The final structure is very well-defined and the resolution is comparable to that of a diamagnetic protein of similar size.[23] This may be attributed to the high number of observed NOEs (an average of 19 per residue). No residues, other than Ala 1, Ser 2, and Pro 25, display less than five interresidue NOEs. As expected, a

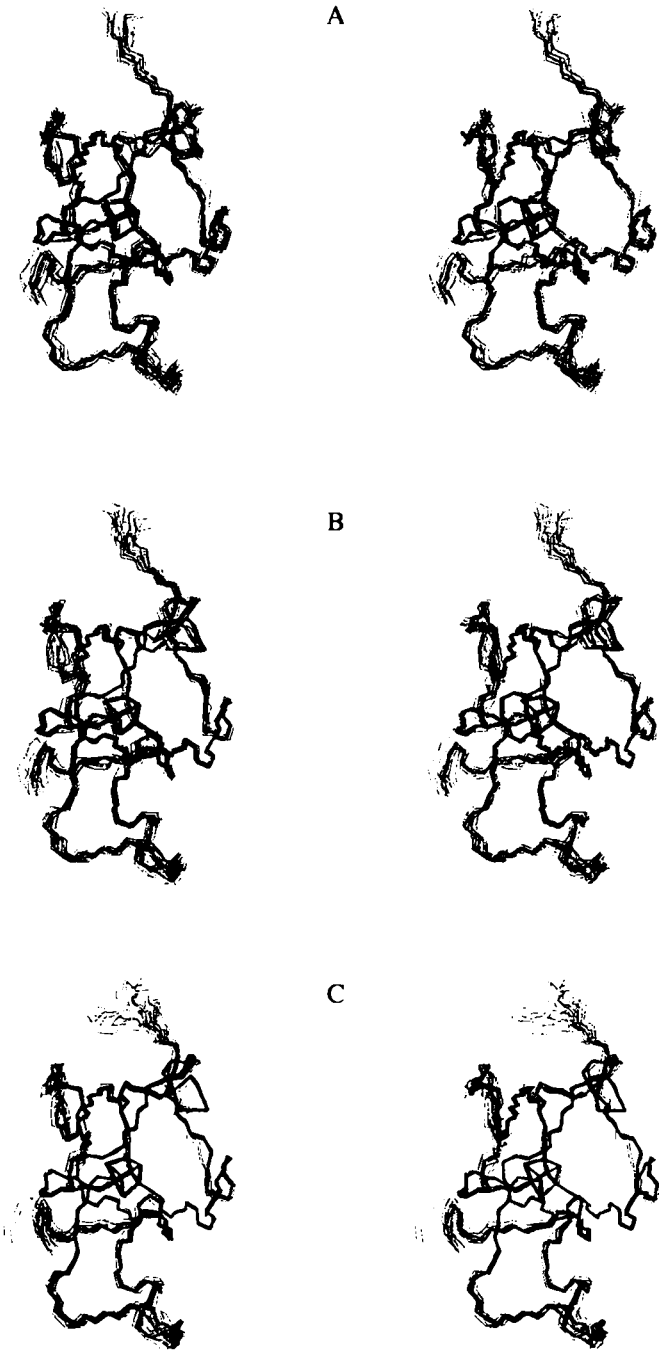

Fig. 3. Stereo drawings of the 18 accepted structures obtained after DG (A), REM (B), and RMD (C) calculations. Structures were aligned by best-fit superimposition of C, Cα, and N atoms of residues 4–71.

0947-6539/95/0109-0600 $ 10.00+.25/0 Chem. Eur. J. 1995, 1, No. 9

slight decrease of the RMSD occurs during the various steps of the refinement (from DG to RMD), though more for the backbone atoms than for all heavy atoms.

Figure 4 shows the RMSD values per residue, for the backbone and for all heavy atoms, calculated for the three families. Lower precision occurs in the region spanning residues 22–30,

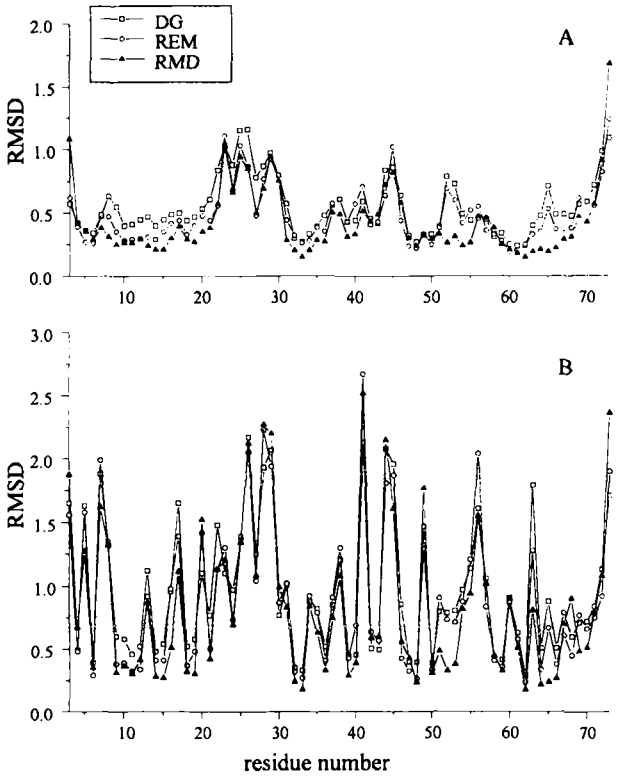

Fig. 4. Backbone (A) and all heavy-atom (B) RMSD per residue within the 18 accepted structures of the DG (□), REM (○), and RMD (▲) families.

due to the fortuitous overlap of several NH resonances of residues of this region at the temperatures used in this study. This overlap reduces the number of constraints. In the DG family, RMSD values higher than average are also observed at residues 44–45, 52–53, and around residue 65. The occurrence of some disorder at residues 44–45 may be attributed to the fact that these residues form a tight turn in a very peripheral region of the protein, and thus almost no long-range connectivities are observed from these residues. The increased RMSD at positions 52–53, as well as at position 65, arises because of the occurrence of two different backbone conformations. Refinement through RMD is particularly efficient in the C-terminal region, especially for those residues where the backbone conformation is not uniquely defined after DG calculations. Residues 52–53 and residue 65 show significant decreases in RMSD in the RMD structures (versus the DG structures) because, of the two possible backbone conformations that satisfy the experimental constraints, the one with lowest energy is selected. By contrast, the RMSD of the residues 22–30 and 44–45 remains high after RMD.

The quality of the structures can be further judged by the order parameter S.[24] This parameter ranges from 1 (univocally defined dihedral angle within the family) to 0 (completly random distribution of the dihedral angle). The $1-S$ values for the ψ (N_i-$C\alpha_i$-CO_i-N_{i+1}) and χ_1 (N_i-$C\alpha_i$-$C\beta_i$-$X\gamma_i$) dihedral angles in each of the calculated families are reported in Figure 5. In the

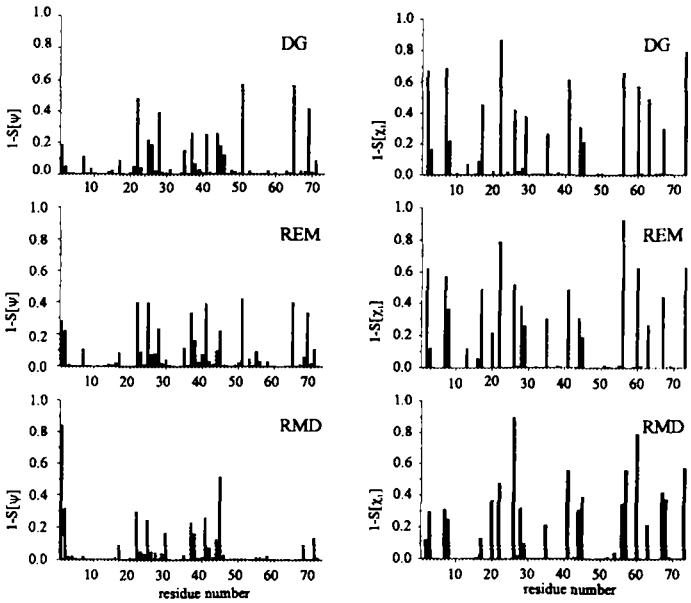

Fig. 5. Plot of the $1-S$ parameter per residue within the 18 accepted structures of the DG, REM, and RMD families for ψ (left) and χ_1 (right) dihedral angles.

DG family there are five residues that show high $1-S$ values for the ψ angle, indicative of ambiguous backbone orientation: His 22, Gln 28, Thr 51, Trp 65, and Tyr 69. For the latter four residues, the structure adopts a single energetically favored conformation during the RMD. The disorder in the region spanning residues 22–30, as measured by possible conformations, is also reduced after RMD. On the other hand, it is interesting that an increase in the disorder of the ψ dihedral angles occurs for residue 45. This could be due to an absence of energetically efficient restraints (steric hindrance, H-bonds, etc.) arising from the peripheral position of the tight turn formed by residues 44–47. Overall, the $1-S$ parameters of the ψ dihedral angles demonstrate that the backbone is very well defined, apart from some disorder in the regions spanning residues 22–30 and 37–46.

Comparison of the structures of the oxidized and reduced proteins: Within the DG families, the structure of the oxidized HiPIP has a higher resolution than that of the reduced protein,[1] with the exception of regions spanning residues 22–30 and 41–46. As an example Figure 6 shows that the aromatic residues surrounding the cluster are better defined in the structure of the oxidized (B) than in that of the reduced protein (A). This is unexpected given the increased paramagnetism of the oxidized cluster ($\mu_{eff} \approx 1.8\,\mu_B$ per iron atom at room temperature)[25] compared to the reduced cluster ($\mu_{eff} \approx 0.8\,\mu_B$ per iron atom at room temperature).[26] The ratio between the number of NOEs observed in the oxidized and reduced forms for each residue is given on a logarithmic scale in Figure 7. The increase in NOEs upon oxidation of the protein is particularly evident in the regions spanning residues 31–39 and 50–65. Overall, the larger number of NOEs observed in the oxidized protein is consistent with the observation that non selective T_1 values measured for Cys protons are smaller in the reduced protein than in the oxidized one.[14]

The structures of the oxidized and of the reduced forms of the protein are very similar in that no major differences in the backbone folding or in any side chain are observed. This is consistent with the notion that there are no major changes in nuclear coordinates coupled to electron transfer.[3, 4, 27] Furthermore,

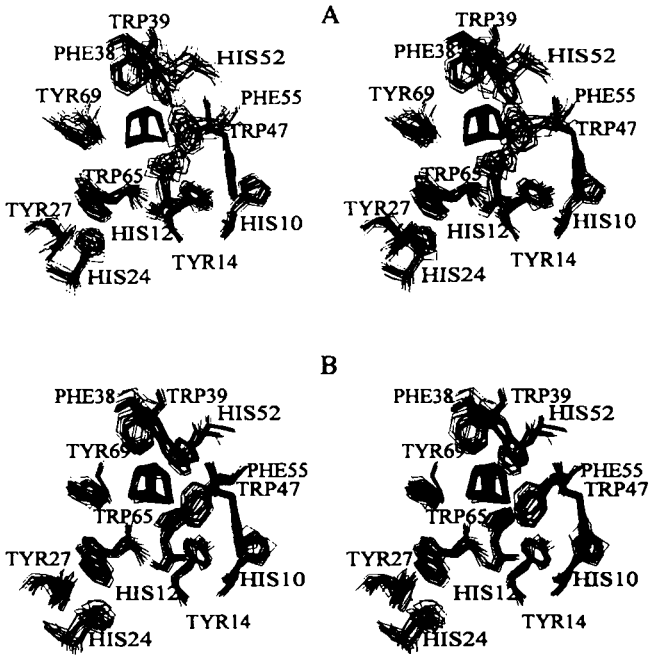

Fig. 6. Stereo drawings of the aromatic residues surrounding the cluster in the DG families of the reduced (A) and of the oxidized (B) forms.

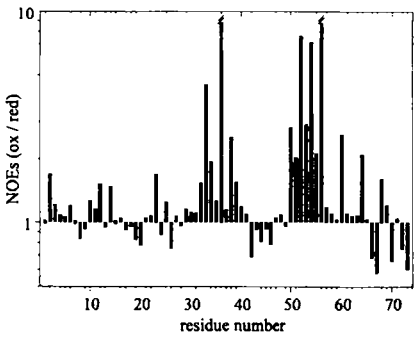

Fig. 7. Ratios between the number of NOEs observed in the oxidized and reduced forms of the protein reported on a logarithmic scale versus the residue number. No NOEs for residues 36 and 56 were observed in the reduced form.

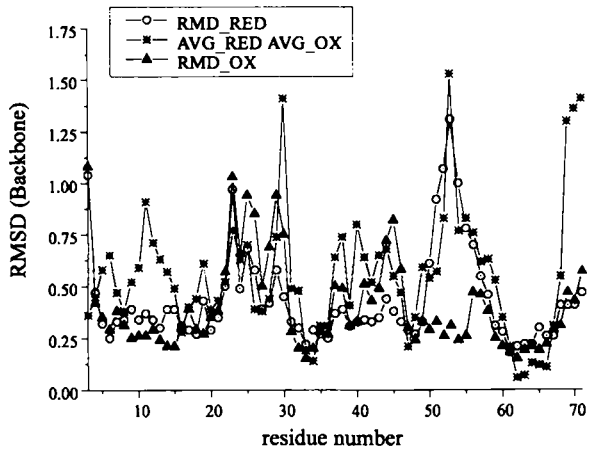

Fig. 8. Plot of the backbone RMSD values per residue within the oxidized (▲) and the reduced (○) RMD families and between the averaged RMD structures of these two families (*).

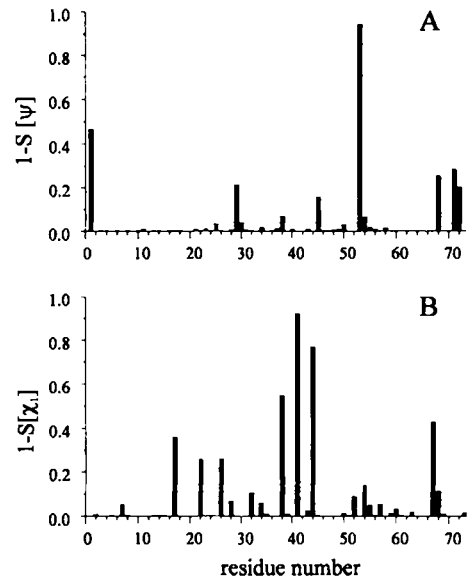

Fig. 9. Plot of the $1-S$ parameter per residue, for ψ (A) and χ_1 (B), between the average structures of the oxidized and of the reduced RMD families.

small differences in the structures of the oxidized and reduced proteins must be interpreted within the limits of the resolution of the structures. To have an idea of the differences between the two forms that are outside experimental error, we report in Figure 8 the RMSD values per residue within the RMD families in the two oxidation states and the RMSD between the average structures of each family. Significant differences between the structures of the two oxidation states are observed for residues 6, 9–15, and 37–38, in the extended region encompassing residues 50–56, and for residues 69–71. Besides these peak values, the RMSD values between the averaged RMD structures of the oxidized and reduced proteins are below 0.7 Å, and the backbones of the two RMD families are superimposable within the error margins. Each of these differences is discussed in detail below.

The difference between the structures at residues 9–15 (a difference maintained in the RMDw structures) arises from a translational movement of this part of the backbone rather than from different folding, as shown by the small value of the $1-S$ parameter for the angle ψ between the averaged structures of the RMD families in the two oxidation states (Fig. 9). The observed effect is not reflected in the aromatic ring of Tyr 14, which is an invariantly conserved residue in all HiPIPs isolated up to now.[28–31] At the present degree of resolution, no movement is observed for the aromatic ring of Tyr 14, although, as it will be pointed out later, the sizable difference in chemical shift for the hydroxyl proton of Tyr 14 observed between the two oxidation states underlines that subtle differences, beyond the resolution of our structures, might occur. Consistent with the above findings, no differences were found for the H-bonding pattern in the close proximity to this residue.

The region around residue 53 is well defined in the structure of the oxidized HiPIP (RMSD < 0.7 Å for residues 50–55), but is poorly defined in the structure of the reduced protein (Fig. 8), thus precluding a meaningful comparison of the structures in this region.

The structural differences observed involving residues 37–38 could arise either from a real structural difference or from the the small number of constraints occurring in this region in both oxidation states.

The DG family of structures of the oxidized and reduced proteins are similar at the C-terminal residues Tyr 69–Pro 71 in that two possible conformations at position 69 are observed and

0947-6539/95/0109-0602 $ 10.00+.25/0 Chem. Eur. J. 1995, 1, No. 9

the CO group of Val 68 is not well defined. Application of RMD causes the family of structures of each oxidation state to converge to unique, but different, conformations. Thus, after the RMD step, the Val 68–Tyr 69 CONH group shows an oxidation state dependent conformation. This difference most probably arises from the electrostatic properties of the cluster in its different oxidation states, and it is therefore sensitive to the choice of the force-field parameters. RMD calculations performed with a different charge distribution (D. A. Case, personal communication) show that the described effect is much less apparent.

When the backbone atoms of the oxidized and reduced families are superimposed, the cluster is observed to be in slightly different orientations in the two states. It is possible that this effect is within the experimental error at the present degree of refinement.

Comparison of ^{1}H and ^{15}N NMR chemical shifts in the two oxidation states: The differences in chemical shifts between the oxidized and reduced *E. halophila* HiPIP I are reported in Figure 10. The data indicate that while chemical shifts for most of the protein are essentially unaffected by the change in oxidation state, there are some regions that are particularly sensitive to the change in the charge of the prosthetic group. This is the case for a region of about four residues centered at Tyr 14, a region spanning residues 33–39, and for most of the residues of the C-terminal portion of the protein (starting from Cys 50). These differences will be discussed below in the comparison of the current data to those of *C. vinosum* HiPIP.

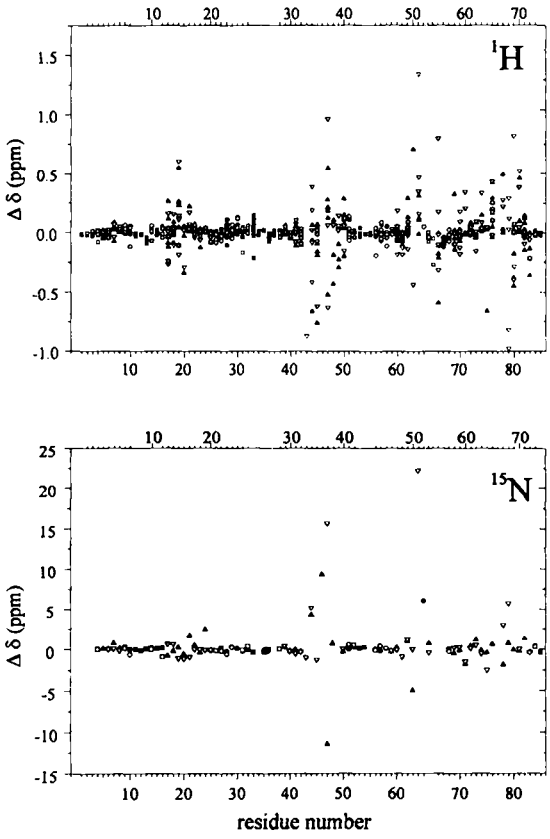

Fig. 10. Observed differences in chemical shift, in the ^{1}H (top) and ^{15}N (bottom) NMR spectra, between the oxidized and the reduced states for both *E. halophila* (hollow symbols) and *C. vinosum* (filled symbols). The alignment is based on the three-dimensional homology. The symbols v and ▲ represent regions of conserved or superimposable residues, □ and ■ insertions, deletions, or regions that are structurally very different, and o and ● residues that are not superimposable but occupy similar regions in space.

It is particularly instructive to report the observed chemical shift differences between the oxidized and the reduced forms ($\Delta\delta$(ppm) = δ_{ox}(ppm)–δ_{red}(ppm)), as a function of the distance of the proton (or nitrogen) to the closest metal (Fig. 11).

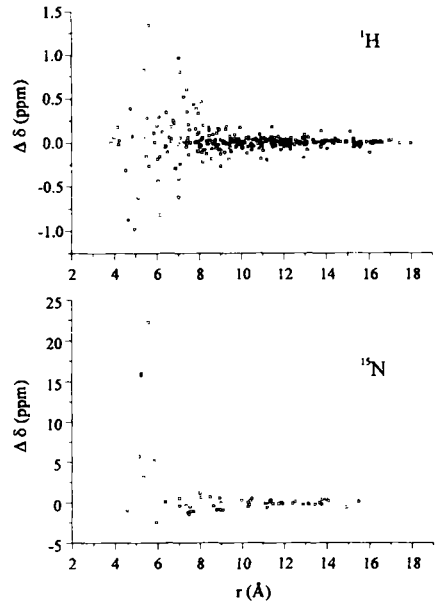

Fig. 11. Observed differences in chemical shift between the oxidized and reduced forms of HiPIP I from *E. halophila* reported as a function of the distance from the closest iron ion.

Considering that several of the resonances arising from protons (or nitrogens) within 6 Å of an iron ion are missing, presumably due to hyperfine interactions and consequent line broadening, the reported data show a remarkable correlation between $\Delta\delta$(ppm) and distance to the nearest iron. These data suggest that the change in the net charge of the prosthetic group affects chemical shifts of the resonances close to it and that this effect does not depend on distance in an isotropic way. If we consider the amide nitrogens and compare their $\Delta\delta$(ppm) values with those of the corresponding proton resonances, we note that there are five amide nitrogens that experience dramatically different chemical shifts in the reduced versus the oxidized protein: Glu 34 (+ 5.2), Ala 37 (+15.8), Thr 51 (+ 22.2), Ser 67 (< ≥ + 4.3), and Val 68 (+ 5.7). The differences in shift observed for these residues are 10 to 100 times larger than those of other amide nitrogens in similar proximity to the cluster. Hence, it is likely that changes in chemical shift arise by more than one mechanism. For each of these amide groups, the corresponding proton signal is shifted by less than 1 ppm; this indicates that the observed $\Delta\delta$(ppm) cannot originate from a pseudocontact contribution. As four of the five affected residues follow a cysteine ligand, a contact contribution from the Cys residues is possible. The absence of data on three of the four Cys amide resonances prevents a full evaluation of this possibility. Nevertheless, in the case of Cys 33–Glu 34, a difference in $\Delta\delta$ of + 5.2 ppm is observed for N of Glu 34 in the oxidized versus the reduced protein, while the equivalent value for N Cys 33 is $\Delta\delta = -1$ ppm (i.e., it is smaller and of opposite sign). As there are three covalent bonds between Cys 33 Sγ and Cys 33 N and four covalent bonds between Cys 33 Sγ and Glu 34 N, a sizable contact contribution to the chemical shift seems very unlikely.

Overall, the ^{1}H and ^{15}N NMR data suggest that the observed differences in the chemical shifts of the oxidized and reduced HiPIP are predominantly diamagnetic in nature. Differences in

chemical shifts upon redox reactions are observed in cytochrome c and in some of its mutants. They are usually ascribed to changes in hydrogen-bonding patterns and, more generally, to alterations of secondary structure elements.[32, 33] While some of the observed changes in chemical shifts may have a similar origin, it is difficult to relate changes of this type to specific structural changes. On the other hand, removal of a unit charge from the cluster upon oxidation may affect electron densities in the neighboring atoms, in turn affecting the corresponding shielding tensor. This is particularly true for heteronuclei. Recent theoretical work has related the reduction potential of the cubane clusters to the number and orientation of the CONH dipoles in the proximity of the cluster itself.[34] The corollary of this may also be true, that is, that the change of a unit charge on the cluster may alter the electronic distribution over the CONH dipoles. According to this reasoning, protons would be affected to a much lesser extent, consistent with the current observations. Differences of this kind have also been observed for cytochromes and were attributed to structural differences.[32, 33] In the present case it seems more likely that differences in chemical shift arise from a change in electronic distribution rather than geometric variations arising from a change in the oxidation state.

Comparison with X-ray data: Comparison of the RMDw structures of the protein in both oxidation states with the two independent molecules observed in the X-ray structure[35] affords a better analysis of the results obtained. Again, interpretation of the RMDw structures is always subject to the relative disorder of the various regions; any observed structural inequalities between the solution structures in the two oxidation states or between one of the solution structures and the X-ray data that occurs within a region characterized by large RMSD in the DG or RMD families must be interpreted with great caution.

Table 3 summarizes the average RMSD values from the pairwise comparison of the RMDw structures of the oxidized and reduced proteins, of the two independent crystal structures, and of the average structures of the DG families of the oxidized and reduced proteins. The RMSD values per residue are reported in Figure 12. Two features are evident: First, the RMDw structures of both the oxidized and reduced HiPIP are slightly more similar to molecule B than to molecule A derived from the crystallographic data. Second, the crystallographic structures are more similar to the solution structure of the reduced HiPIP than

Table 3. Pairwise average RMSD for the RMDw structures (oxidized and reduced), for the two X-ray molecules, and for the average structures of the oxidized and reduced DG families. Values reported in the upper part of the table were obtained by best-fit superimposition of backbone atoms for residues 3–71; those reported in the lower part were obtained by considering residues 3–21 and 30–71.

	X-ray A	X-ray B	RMDw Ox	RMDw Red	DG Ox	DG Red
X-ray A		BB 0.49 HA 1.23	BB 1.30 HA 2.20	BB 0.75 HA 1.65	BB 0.95 HA 1.50	BB 0.85 HA 1.42
X-ray B	BB 0.50 HA 1.18		BB 1.16 HA 1.89	BB 0.69 HA 1.54	BB 0.86 HA 1.46	BB 0.78 HA 1.35
RMDw Ox	BB 0.97 HA 1.68	BB 0.87 HA 1.66		BB 0.99 HA 1.56	BB 0.85 HA 1.40	BB 1.11 HA 1.68
RMDw Red	BB 0.72 HA 1.53	BB 0.67 HA 1.46	BB 0.77 HA 1.37		BB 0.68 HA 1.40	BB 0.68 HA 1.21
DG Ox	BB 0.93 HA 1.47	BB 0.85 HA 1.40	BB 0.64 HA 1.16	BB 0.68 HA 1.32		BB 0.71 HA 1.11
DG Red	BB 0.85 HA 1.40	BB 0.79 HA 1.34	BB 0.83 HA 1.39	BB 0.67 HA 1.16	BB 0.70 HA 1.08	

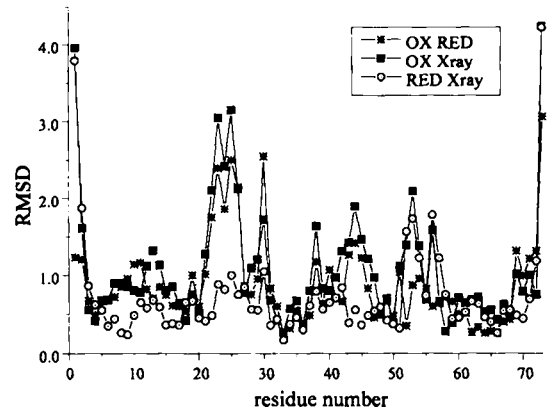

Fig. 12. Pairwise RMSD per residue between the oxidized and the reduced RMDw structures (*), between the oxidized RMDw structure and the solid-state structure (molecule B) (■), and between the reduced RMDw structure and the solid state structure (molecule B) (○).

to that of the oxidized protein. These relative similarities are discernible in the DG structures, but are more pronounced after RMDw refinement. The two RMDw structures together with the crystallographic structure of molecule B are presented in Figure 13. The largest variation in these structures occurs in the

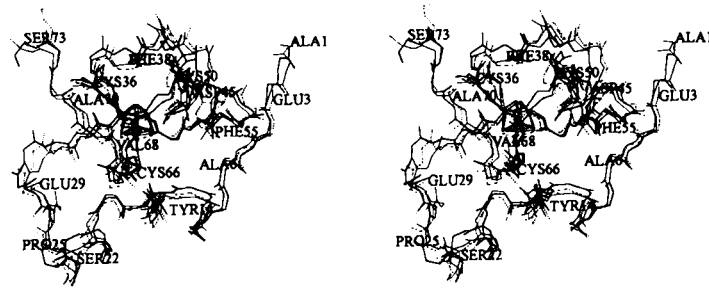

Fig. 13. Stereo drawing of the backbone atoms of the solid-state structure (molecule B, dashed line) superimposed on the RMDw structure of the oxidized form (thick line) and the RMDw structure of the reduced form (thin line). Structures were aligned by best-fit superimposition of C, Cα, and N atoms of residues 4–71.

region spanning residues 22–30, where the resolution of the solution structure of the oxidized protein is lower. The similarities of the three structures were reevaluated omitting this region to avoid bias from the lower resolution. Even if the RMSD values of the oxidized protein are decreased by 25% (Table 3, lower half vs. upper half), the crystal structure (molecule B) remains more similar to the solution structure of the reduced HiPIP than to that of the oxidized protein. For the *C. vinosum* HiPIP, the crystallographic structure of the protein is also more similar to the solution structure of the reduced protein .[2, 7, 18]

Of particular note is the increased distance between His 52 NH and Cys 50 Sγ in both solution structures relative to the crystallographic structure. This increased distance is sufficient to prevent the formation of an H-bond between His 52 HN and Cys 50 Sγ. On the other hand resonance Raman experiments performed on *C. vinosum* HiPIP[36] have shown that the amide proton of Leu 65, which is roughly superimposable with His 52 of *E.* halophila HiPIP I, forms an NHS hydrogen bond with a cysteine sulfur atom. Unfortunately, no signal corresponding to His 52 HN was detected in the protein in either oxidation state, thus precluding the direct monitoring of the dipolar connectivities of His 52 HN and changes in chemical shift experienced by His 52 backbone resonances when passing from the oxidized to the reduced state.

0947-6539/95/0109-0604 $ 10.00+.25/0 Chem. Eur. J. 1995, 1, No. 9

Comparison of the solution structures of oxidized and reduced *C. vinosum* HiPIP and *E. halophila* HiPIP I: From the above discussion, it is clear that while most of the protein is unaffected by the change in redox state, there are some regions that may have a redox state dependent conformation. This finding is of particular interest in the light of the recently solved solution structures of oxidized and reduced *C. vinosum* HiPIP.[2, 7] The high homology between the structures of the two proteins, as established from X-ray data[17, 18] and extensively discussed by Holden and co-workers,[37] extends to the statistical parameters and to possible redox state dependent conformations. The analogies between the structures of *E. halophila* HiPIP I and *C. vinosum* HiPIP in the two redox states are summarized below:

1) In the oxidized proteins, T_1 values of the hyperfine-shifted signals are longer, the assignment is more extensive, and the observed number of NOEs increases. Thus, although paramagnetism is higher in the oxidized form ($S = {}^1/_2$ ground state, instead of $S = 0$), $[Fe_4S_4]^{3+}$ HiPIPs are more suitable for NMR investigations than $[Fe_4S_4]^{2+}$ HiPIPs.
2) Due to the increased number of constraints that are obtained for the oxidized proteins, the quality of the structure of the oxidized protein, as judged by the RMSD values and the $1-S$ parameter for dihedral angles, is higher than that of the reduced protein at each of the three refinement levels (DG, REM, and RMD).
3) The X-ray structures are more similar to the solution structures of the corresponding reduced proteins than to those of the oxidized proteins. This is true although the available X-ray structure of *C. vinosum* HiPIP is of the oxidized protein.[18] The oxidation state of the crystallized *E. halophila* HiPIP I was not specified.[17]
4) Other than some translational movements, the structure of the regions spanning the residues 1–20 in *E. halophila* HiPIP I (corresponding to 1–25 in *C. vinosum* HiPIP) and residues 57–65 in *E. halophila* (68–76 in *C. vinosum*) are very similar in both oxidation states and very similar to the corresponding X-ray structure.
5) The regions showing differences, either between the solution structures of the oxidized and reduced proteins or between the solution and crystallographic structures, are amazingly similar for the two proteins. In most cases these differences may be exaggerated by the lower number of constraints in these regions; thus, it is difficult to pinpoint specific structural differences. Nevertheless, these differences are conserved in the three-dimensional alignment and for the most part involve aromatic residues (Phe 38 (Phe 48), His 52 (Leu 65), and Phe 55 (Phe 66)).
6) The chemical shift differences observed between oxidized and reduced forms are also surprisingly similar for *both* proteins. Figure 10 reports also the chemical shift differences on the basis of the proposed three-dimensional alignment of the sequences.[17, 29] No redox state dependent differences in chemical shifts are observed in the external parts of the proteins. Significant differences are noted, as the backbone approaches the cluster, at residues 33–41 (43–51 for *C. vinosum*, and encompassing Cys I and Cys II[38]), 49 (62 in *C. vinosum*), 51 (Gln 64 for *C. vinosum*, close to Cys III) and from residue 58 (69 for *C. vinosum*) to the C terminal of the protein. Tyrosine 14 and phenylalanine 55 (Tyr 19 and Phe 66, respectively, for *C. vinosum*) also approach the cluster with their side chains (less than 3.5 Å from a ring proton to a S of Cys ligand or from an S of the cluster) and experience differences in chemical shifts. These two residues are of particular interest and, except for Phe 55 in *R. tenuis* HiPIP,[39] they are conserved in all HiPIPs that have been isolated to date. In the case of Tyr 14, an interaction between the aromatic ring and the lone pair of S of cysteine has been proposed to be a possible determinant of the electron transfer properties of the protein.[18] The ring of Phe 55 has been observed to be in different orientations with respect to the cluster in different HiPIPs.[17, 18] In the present structures Phe 55 could also experience the same kind of interaction.

The electron transfer rearrangement in related proteins: Cytochromes constitute good probes to study whether structural rearrangements are observed upon changing the oxidation state. In the early 1980's, X-ray data on ferrocytochrome c and ferricytochrome c at a resolution of 1.5 Å and 1.8 Å, respectively,[27, 40] revealed that structural changes occur involving residues close to the heme pocket, namely, Tyr 67, Asn 52, Tyr 48, and a water molecule. The heme was found to be flatter in the oxidized state. NMR studies based solely on the analysis of proton chemical shifts and NOE intensities of WT and mutated cytochromes c in the two redox oxidation states revealed that the change in redox state is coupled to a rearrangement of the H-bond network that runs through the protein.[41] This is consistent with the X-ray studies. However, more recently, X-ray data on the two oxidation states of yeast iso-1-cytochrome c showed that the overall average value for the differences in the main-chain atoms is 0.31 Å, whereas all H-bond interactions between main-chain residues are retained.[42] One of the most significant redox state dependent conformational differences involve a water molecule (WAT 166) that is displaced 1.7 Å towards the heme iron in the oxidized state. It has been proposed that this water molecule stabilizes both oxidation states by a number of mechanisms; the disruption of interactions mediated by WAT 166 can decrease the redox potential by 56 mV.[43] More thorough NMR studies and their interpretation may shed further light on these systems.

The blue copper proteins are an important class of electron transfer proteins.[44] They cannot be studied by NMR in the oxidized state because copper(II) has an unfavorable electron relaxation time.[45] From X-ray studies[46, 47] it is apparent that only minor variations in bond lengths and angles are observed. In plastocyanin, a lengthening of the two Cu–N(His) bonds by about 0.1 Å was observed upon reduction, together with a 10° degree variation in the Cu-S-Cβ(Cys) bond angle.[47] Also other small variations involving the polypeptide chain were observed, but they were too small to be associated to a functional role.[47]

Concluding Remarks

We have solved the three-dimensional structure in solution of the paramagnetic protein HiPIP I from *E. halophila* in the oxidized state. The quality of the structure obtained is higher than for the reduced form of this protein and for the solution structure of *C. vinosum* HiPIP in both oxidation states. It is always interesting to note that, although the ^{1}H NMR spectra of the oxidized and reduced proteins are rather different, the structures obtained are amazingly similar. A comparison of the RMSD values for the oxidized and reduced structures indicates that they are not equal. Minor differences are observed in several protein parts. However, better resolution is needed for a more detailed analysis. The observed differences in chemical shifts between the two oxidation states reflect changes in the electronic structure, possibly with a contribution from minor geometrical changes. The behavior observed for *E. halophila* HiPIP I can be compared to that observed for *C. vinosum* HiPIP. When the

  0947-6539/95/0109-0605 $ 10.00+.25/0

chemical shifts of the two proteins are compared on the basis of their sequence homology and of their three-dimensional alignment, it can be concluded that the reorganization resulting from electron transfer, as monitored by the chemical shifts, is similar in the two proteins. In the above discussion, this behavior has been compared with that of other systems studied previously by NMR spectroscopy or other techniques.

Experimental Procedure

Sample preparation: A sample of purified recombinant *E. halophila* HiPIP I was obtained as previously described [48]. The recombinant protein differs from the native one in that it has two additional N-terminal amino acids, designated as Ala 1 and Ser 2. About 15 mg of the protein, as obtained from the last purification step (4-morpholinepropanesulfonic acid (MOPS), pH = 7, 0.1 M NaCl), was exchanged by ultrafiltration (Amicon YM 3 membrane) into 50 mM phosphate (pH = 5.0). The protein was maintained in the oxidized state by the addition of 2.5 μL of a 0.1 M solution of $K_3[Fe(CN)_6]$ in 50 mM phosphate. D_2O was added to a final concentration of 10% for the deuterium lock. The sample had a final volume of 500 μL and protein concentration of 3.5 mM. Protein samples dissolved in D_2O were prepared by using analogous solutions of D_2O. The ^{15}N-labeled HiPIP was isolated and purified from *E. coli* cultures grown in a minimal medium (M9) enriched with $(^{15}NH_4)_2SO_4$ (0.6 $g L^{-1}$).

NMR spectroscopy: NMR spectra were recorded on a AMX600 Bruker Spectrometer at two different temperatures (288 and 298 K). Hyperfine-shifted signals were recorded over a spectral window of 125 kHz. The ^1H NMR spectrum of the protein recorded over a 125 kHz spectral window is reported elsewhere [14], together with the assignment of the hyperfine-shifted signals belonging to βCH_2 and αCH protons of Cys residues. 1 D NOEs were performed on the nine signals (seven of which were affected by a sizable hyperfine shift) that could be selectively irradiated by using the superWEFT pulse sequence (180-τ-90-aq-RD) [49]. Selective irradiation was accomplished by a selective decoupler pulse during the delay τ, as described previously [50·51]. Irradiation times were varied from 20 ms to 170 ms in order to discriminate betwee first- and second-order NOEs. Furthermore, the experiments were repeated with two different spectral windows. In one series of 1 D NOEs, the spectral window was maintained at 125 kHz to quantitatively estimate the observed NOEs with respect to the irradiated signal. In the second series of experiments, measurements were collected over a spectral window of 8.6 kHz and 8192 data points, to achieve a higher resolution. The latter procedure allowed a more accurate analysis of the connectivities observed in the diamagnetic region. Finally, a NOESY [52] using a spectral window of 85 kHz and 1024 data points in F2 (356 experiments) was recorded at 288 K. Mixing and recycle delays of 9 ms and 62 ms, respectively, were used. The spectral window was further minimized by placing the carrier frequency at $\delta = 36.3$ and presaturating the water signal by using an off-resonance DANTE sequence [53].

Signals within the diamagnetic envelope were recorded by a variety of techniques. NOESY spectra with mixing times of 100 ms and clean-TOCSY spectra [54] with spin lock times of 25 ms were recorded both in H_2O and D_2O at two different temperatures (288 and 298 K). A NOESY spectrum obtained with a mixing time of 15 ms and a TOCSY spectrum with a spin lock time of 10 ms were recorded on the D_2O sample at 288 K. 4096 data points were collected in the acquisition dimension, and 900–975 experiments were acquired in the other dimension, except in the case of the NOESY and TOCSY experiments with short mixing times, for which 742 and 536 experiments were acquired, respectively. Quadrature detection was achieved either with the States method [55] or with the TPPI method [56]. The water signal was suppressed through presaturation during the mixing time and the relaxation delay. Raw data were processed with the standard Bruker software. Data in the time domain were zero-filled in order to obtain 2 K × 1 K data points in the frequency domain. A polynomial baseline correction and a squared cosine apodization function were applied in both dimensions. HMQC experiments [57·58] were performed on a sample of ^{15}N-labeled protein in a 5 mm reverse detection probe. Proton chemical shifts were calibrated by assigning the H_2O or HDO signal shift values of 4.81 and 4.93 ppm from sodium 4,4-dimethyl-4-silapentane-1-sulfonate (DSS) at the temperatures of 298 and 288 K, respectively. Nitrogen chemical shifts were calibrated by assigning the $(^{15}NH_4)_2SO_4$ signal a shift of 21.6 ppm at 298 K, referenced to liquid ammonia. All spectra were analyzed with the aid of the program XEASY [59] on IBM RISC 6000/530 computers.

Distance geometry calculations: Intensities of dipolar connectivities in all 2D NOESY spectra obtained using a 100 ms mixing time (for samples in H_2O or D_2O, recorded at either temperature) were measured using the integration routines in the program XEASY [59]. Where peaks strongly overlapped, contributions from the individual peaks were estimated by fitting the overall intensity to the line shapes determined from the 2 D spectrum [60]. Peak volumes were converted into distance constraints with the program CALIBA [16]. NOEs were divided into five different classes: 1) intraresidue except HN, Hα, Hβ; 2) sequential and intraresidue HN, Hα, Hβ; 3) medium range; 4) long range backbone; and 5) long range. Connectivities obtained through steady-state or truncated NOE experiments where transformed into upper distance limits by a different calibration procedure, described earlier.

The three-dimensional structures were calculated with the distance geometry (DG) program DIANA [16] employing the redundant angle constraint strategy (REDAC) [19]. A preliminary REDAC cycle was used to determine redundant angle constraints. These redundant angle constraints, together with experimental distance constraints, were used on 500 random starting conformations. Cutoffs on the target function of 1.2 $Å^2$ in the first step and of 1.0 $Å^2$ in the second and third steps were used to select 29 and 18 structures, respectively. The final DG run was performed without the redundant angle constraints using the 18 structures as starting conformations [19]. These 18 conformers are referred to as the DG family of structures. The cluster was simulated in the distance geometry calculations using the previously described strategy [1]. Stereospecific assignments were achieved through the program GLOMSA [16] in the final stages of the structure calculation.

Molecular dynamics refinement: Restrained energy minimization (REM) and restrained molecular dynamics (RMD) calculations on the structures obtained from distance geometry calculations were performed using the SANDER [22] module of the AMBER 4.0 program package [61]. The force-field parameters for all residues, except the cluster and the cysteine ligands to the irons, were the standard AMBER "all atoms" parameters [62]. For the iron and sulfur atoms and for the iron-bound cysteines, previously reported force-field parameters were used [20·21]. Such parameters differ sizably from those proposed by D. A. Case (personal communication); calculations with the latter parameters provide almost identical results except for residues 68–69. The energy of each of the 18 DG structures was minimized (REM family of structures). Each structure was then subjected to a molecular dynamics simulation of 36.0 ps in vacuo. The system was heated from 0 to 300 K in a coupled thermal bath of 300 K with a time constant of 0.1 ps [63]. A distance-dependent dielectric constant was used. The time step was 1.5 fs. The bond lengths in all RMD calculations were kept rigid by using the SHAKE algorithm [64], whereas they were allowed to vary in all REM calculations. The nonbonded interactions were evaluated with a cutoff of 10 Å, and the pair list was updated every 20 steps. During the calculations, a NOE-weighted potential function [22] was applied by using the SANDER module of AMBER. The mixed linear–harmonic potential is reported elsewhere [1, 22].

The RMD trajectories were analyzed with the program CARNAL [65]. The final 12.0 ps of the RMD simulation of each structure were used to generate an average structure whose energy was again minimized. The 18 structures obtained in this way represent the RMD family. The mean structure of the RMD family was subjected to further MD calculations in water. The procedure is basically the same as the one used for simulations in vacuo except that a 10 Å-thick shell of water molecules, together with six appropriately placed Na^+ ions to neutralize the protein, were added, and a fixed dielectric constant was used. The trajectory was calculated for 144 ps and the last 36 were averaged to obtain the final structure (RMDw structure). All calculations were performed with double-precision accuracy on IBM RISC 600/530 computers.

Acknowledgments: D. K. thanks the European Union, Human Capital and Mobility Program, for a postdoctoral fellowship. This research was in part financially supported by CNR Progetto Finalizzato Biotecnologie e Biostrumentazione, CNR Progetto Finalizzato Chimica Fine, CNR Comitato Scienze Agrarie.

Received: February 20, 1995 [F89]

[1] L. Banci, I. Bertini, L. D. Eltis, I. C. Felli, D. H. W. Kastrau, C. Luchinat, M. Piccioli, R. Pierattelli, M. Smith, *Eur. J. Biochem.* **1994**, *225*, 715–725.
[2] L. Banci, I. Bertini, A. Dikiy, D. H. W. Kastrau, C. Luchinat, P. Sompornpisut, *Biochemistry* **1995**, *34*, 206–219.
[3] R. A. Marcus, N. Sutin, *Biochim. Biophys. Acta* **1985**, *811*, 265–322.
[4] H. B. Gray, W. R. Ellis, Jr., in *Bioinorganic Chemistry* (Eds.: I. Bertini, H. B. Gray, S. J. Lippard, J. S. Valentine), University Science Books, Mill Valley, California, **1994**, p. 315–364.
[5] C. W. J. Carter, J. Kraut, S. T. Freer, R. A. Alden, *J. Biol. Chem.* **1974**, *249*, 6339–6346.
[6] G. M. Clore, A. M. Gronenborn, *Protein Sci.* **1994**, *3*, 372–390.
[7] I. Bertini, A. Dikiy, D. H. W. Kastrau, C. Luchinat, P. Sompornpisut, *Biochemistry*, **1995**, *34*, 9851–9858.
[8] K. Dus, H. De Klerk, K. Sletten, R. G. Bartsch, *Biochim. Biophys. Acta* **1967**, *140*, 291.
[9] P. Middleton, D. P. E. Dickson, C. E. Johnson, J. D. Rush, *Eur. J. Biochem.* **1980**, *104*, 289–296.
[10] D. P. E. Dickson, C. E. Johnson, R. Cammack, M. C. W. Evans, D. O. Hall, K. K. Rao, *Biochem. J.* **1974**, *139*, 105.
[11] I. Bertini, A. P. Campos, C. Luchinat, M. Teixeira, *J. Inorg. Biochem.* **1993**, *52*, 227–234.
[12] I. Bertini, S. Ciurli, C. Luchinat, *Struct. Bonding* **1995**, Vol. 83, p. 1–54.
[13] A. Hochkoeppler, S. Ciurli, G. Venturoli, D. Zannoni, *FEBS Lett.* **1995**, *357*, 70–74.

[14] I. Bertini, F. Capozzi, L. D. Eltis, I. C. Felli, C. Luchinat, M. Piccioli, *Inorg. Chem.* **1995**, *34*, 2516–2523.
[15] K. Wüthrich, *NMR of Proteins and Nucleic Acids*, Wiley, New York, **1986**.
[16] P. Güntert, W. Braun, K. Wüthrich, *J. Mol. Biol.* **1991**, *217*, 517–530.
[17] D. R. Breiter, T. E. Meyer, I. Rayment, H. M. Holden, *J. Biol. Chem.* **1991**, *266*, 18660–18667.
[18] C. W. J. Carter, J. Kraut, S. T. Freer, N.-H. Xuong, R. A. Alden, R. G. Bartsch, *J. Biol. Chem.* **1974**, *249*, 4212–4215.
[19] P. Güntert, K. Wüthrich, *J. Biomol. NMR* **1991**, *1*, 447–456.
[20] L. Banci, I. Bertini, F. Capozzi, P. Carloni, S. Ciurli, C. Luchinat, M. Piccioli, *J. Am. Chem. Soc.* **1993**, *115*, 3431–3440.
[21] L. Banci, I. Bertini, P. Carloni, C. Luchinat, P. L. Orioli, *J. Am. Chem. Soc.* **1992**, *114*, 10683–10689.
[22] D. A. Pearlman, D. A. Case, *SANDER: University of California*, San Francisco, **1991**.
[23] *Macromolecular Structures*, Current Biology, London **1993**.
[24] S. G. Hyberts, M. S. Goldberg, T. F. Havel, G. Wagner, *Protein Sci.* **1992**, *1-I*, 36–751.
[25] T. H. Moss, D. Petering, G. Palmer, *J. Biol. Chem.* **1969**, *244*, 2275-2277.
[26] W. D. Phillips, C. C. McDonald, N. A. Stombaugh, W. H. Orme-Johnson, *Proc. Natl. Acad. Sci. USA* **1974**, *71*, 140–143.
[27] T. Takano, R. E. Dickerson, *J. Mol. Biol.* **1981**, *153*, 95–155.
[28] S. M. Tedro, T. E. Meyer, M. D. Kamen, *J. Biol. Chem.* **1976**, *251*, 129–136.
[29] S. M. Tedro, T. E. Meyer, R. G. Bartsch, M. Kamen, *J. Biol. Chem.* **1981**, *25*, 731.
[30] C. T. Przysiecki, T. E. Meyer, M. A. Cusanovich, *Biochemistry* **1985**, *24*, 2542–2549.
[31] R. P. Ambler, T. E. Meyer, M. D. Kamen, *Arch. Biochem. Biophys.* **1994**, *308*, 78–81.
[32] Y. Gao, J. Boyd, G. J. Pielak, R. J. P. Williams, *Biochemistry* **1991**, *30*, 7033–7040.
[33] Y. Gao, J. Boyd, R. J. P. Williams, G. J. Pielak, *Biochemistry* **1990**, *29*, 6994–7003.
[34] G. M. Jensen, A. Warshel, P. J. Stephen, *Biochemistry* **1994**, *33*, 10911–10924.
[35] A more refined X-ray structure of this protein has been recently produced (Holden, personal communication) but is not available in the literature.
[36] G. Backes, Y. Mino, T. M. Loehr, T. E. Meyer, M. A. Cusanovich, W. V. Sweeney, E. T. Adman, J. Sanders-Loehr, *J. Am. Chem. Soc.* **1991**, *113*, 2055–2064.
[37] M. M. Benning, T. E. Meyer, I. Rayment, H. M. Holden, *Biochemistry* **1994**, *33*, 2476–2483.
[38] Cysteine residues, in *E. halophila* and of *C. vinosum*, are sometimes referred to according to the increasing number in the sequence, as Cys I, Cys II, Cys III, and Cys IV.
[39] I. Rayment, G. Wesemberg, T. E. Meyer, M. A. Cusanovich, H. M. Holden, *J. Mol. Biol.* **1992**, *228*, 672.
[40] T. Takano, R. E. Dickerson, *J. Mol. Biol.* **1981**, *153*, 79–94.
[41] Y. Gao, G. McLendon, G. J. Pielak, R. J. P. Williams, *Eur. J. Biochem.* **1992**, *204*, 337–352.
[42] A. M. Berghuis, G. D. Brayer, *J. Mol. Biol.* **1992**, *223*, 959–976.
[43] A. M. Berghuis, J. G. Guillemette, G. McLendon, F. Sherman, M. Smith, G. D. Brayer, *J. Mol. Biol.* **1994**, *235*, 786.
[44] S. K. Chapman in *Perspectives on bioinorganic chemistry* (Eds.: R. W. Hay, J. R. Dilworth, K. B. Nolan), Jai, London, **1991**, pp. 95–140.
[45] L. Banci, I. Bertini, C. Luchinat, *Nuclear and electron relaxation. The magnetic nucleus-unpaired electron coupling in solution*, VCH, Weinheim, **1991**.
[46] J. M. Guss, H. C. Freeman, *J. Mol. Biol.* **1983**, *169*, 521–563.
[47] J. M. Guss, P. R. Harrowell, M. Murata, V. A. Norris, H. C. Freeman, *J. Mol. Biol.* **1986**, *192*, 361–387.
[48] L. D. Eltis, S. G. Iwagami, M. Smith, *Protein Eng.* **1994**, *7*, 1145–1150.
[49] T. Inubushi, E. D. Becker, *J. Magn. Reson.* **1983**, *51*, 128–133.
[50] L. Banci, I. Bertini, C. Luchinat, M. Piccioli, A. Scozzafava, P. Turano, *Inorg. Chem.* **1989**, *28*, 4650–4656.
[51] S. W. Unger, J. T. J. Lecomte, G. N. La Mar, *J. Magn. Reson.* **1985**, *64*, 521–526.
[52] S. Macura, K. Wüthrich, R. R. Ernst, *J. Magn. Reson.* **1982**, *47*, 351–357.
[53] G. A. Morris, R. Freeman, *J. Magn. Reson.* **1978**, *29*, 433–462.
[54] C. Griesinger, G. Otting, K. Wüthrich, R. R. Ernst, *J. Am. Chem. Soc.* **1988**, *110*, 7870–7872.
[55] D. J. States, R. A. Habenkorn, D. J. Ruben, *J. Magn. Reson.* **1982**, *48*, 286–292.
[56] D. Marion, K. Wüthrich, *Biochem. Biophys. Res. Commun.* **1983**, *113*, 967–974.
[57] A. Bax, R. H. Griffey, B. L. Hawkins, *J. Am. Chem. Soc.* **1983**, *105*, 7188–7190.
[58] A. Bax, R. H. Griffey, B. L. Hawkins, *J. Magn. Reson.* **1983**, *55*, 301–315.
[59] C. Eccles, P. Güntert, M. Billeter, K. Wüthrich, *J. Biomol. NMR* **1991**, *1*, 111–130.
[60] T. A. Holak, J. N. Scarsdale, J. H. Prestegard, *J. Magn. Reson.* **1987**, *74*, 546–549.
[61] D. A. Pearlman, D. A. Case, G. C. Caldwell, G. L. Siebel, U. C. Singh, P. Weiner, P. A. Kollman, *AMBER 4.0*, University of California, San Francisco, **1991**.
[62] S. J. Weiner, P. A. Kollman, D. T. Nguyen, D. A. Case, *J. Comp. Chem.* **1986**, *7*, 287–303.
[63] H. J. C. Berendsen, J. P. M. Postma, W. F. van Gunsteren, A. DiNola, J. R. Haak, *J. Chem. Phys.* **1984**, *81*, 3684–3690.
[64] W. F. van Gunsteren, H. J. C. Berendsen, *Mol. Phys.* **1977**, *34*, 1311–1327.
[65] W. S. Ross, *CARNAL*, Department of Pharmaceutical Chemistry, University of California, San Francisco, **1994**.